Ocean Modelling 70 (2013) 75–84

Contents lists available at SciVerse ScienceDirect

Ocean Modelling

journal homepage: www.elsevier.com/locate/ocemod

Modeling wave-mud interaction on the central chenier-plain coast, western Louisiana Shelf, USA

I. Safak [a,*], C. Sahin [b], J.M. Kaihatu [c], A. Sheremet [b]

[a] Department of Environmental Sciences, University of Virginia, 291 McCormick Road, Clark Hall, Charlottesville, VA 22904, USA
[b] Department of Civil and Coastal Engineering, University of Florida, 365 Weil Hall, P.O. Box 116590, Gainesville, FL 32611, USA
[c] Zachry Department of Civil Engineering, Texas A&M University, 3136 TAMU, College Station, TX 77843, USA

ARTICLE INFO

Article history:
Available online 25 November 2012

Keywords:
Wave modeling
Surface waves
Nonlinear waves
Wave dissipation
Muddy seafloor
Mud
Viscosity
Bottom boundary layer
Louisiana Shelf

ABSTRACT

The strong coupling between hydrodynamics and seafloors on shallow muddy shelves, and resulting bed reworking, have been extensively documented. On these shelves, spectral wave transformation is driven by a complex combination of forcing mechanisms that include nonlinear wave interactions and wave energy dissipation induced by fluid-mud at a range of frequencies. Wave-mud interaction is investigated herein by using a previously validated nonlinear spectral wave model and observations of waves and near-bed conditions on a mildly-sloping seafloor off the muddy central chenier-plain coast, western Louisiana Shelf, United States. Measurements were made along a cross-shelf transect spanning 1 km between 4 and 3 m water depths. The high-resolution observations of waves and near-bed conditions suggest presence of a fluid mud layer with thickness sometimes exceeding 10 cm under strong long wave action (1 meter wave height with 7 s peak period at 4 meter depth). Spectral wave transformation is modeled using the stochastic formulation of the nonlinear Mild Slope Equation, modified to account for wave-breaking and mud-induced dissipation. The model is used in an inverse manner in order to estimate the viscosity of the fluid mud layer, which is a key parameter controlling mud-induced wave dissipation but complicated to measure in the field during major wave events. Estimated kinematic viscosities vary between 10^{-4}-10^{-3} m^2/s. Combining these results of the wave model simulations with in-depth analysis of near-bed conditions and boundary layer modeling allows for a detailed investigation of the interaction of nonlinear wave propagation and mud characteristics. The results indicate that mud-induced dissipation is most efficient when the wave-induced resuspensions of concentrations > 10 g/L settle due to relatively small bottom stresses to form a fluid mud layer that is not as thin and viscous as a consolidated seafloor in absence of wave action but also not as thick and soft as a near-bed high concentration layer that forms during strong wave action.

1. Introduction

In nearshore muddy environments, energetic surface waves have been observed to soften the initially consolidated seafloor and cause resuspension of sediment which finally settles to form fluid mud layers (e.g., Jaramillo et al., 2009; Sahin et al., 2012), the thickness of which depends on site-specific mud properties and hydrodynamic conditions. Interaction of waves with these high concentration mud layers causes significant wave energy dissipation (e.g., Sheremet et al., 2005). The dissipation rate was reported to be more significant during the phase of hindered settling of the resuspended material when a fluid mud layer forms (Sheremet et al., 2011a), and dramatically greater than that observed over sandy shelves (e.g., Ardhuin et al., 2003). Mud-induced wave energy dissipation is observed at both low frequencies and at the short wave band of the spectrum. This short wave band is not kinematically coupled to the seafloor; energy loss in this band was hypothesized to be due to nonlinear energy transfers across the spectrum, i.e., triad interactions (Sheremet and Stone, 2003).

An early study of wave propagation on muddy seafloors (Gade, 1958) considered a two-layer system consisting of water overlaying a viscous fluid representing the muddy seafloor. The resulting model of Gade (1958) is valid for long waves; with it, wave heights were seen to exponentially decay as waves propagate. This model was later improved with the inclusion of viscous effects in both layers, and an extension to dispersive waves (Dalrymple and Liu, 1978). An analytical limit to the model of Dalrymple and Liu (1978) was derived by Ng (2000). This simplification is valid when the thickness of the mud layer (h_o) is comparable to the Stokes'

* Corresponding author. Tel.: +1 508 457 23 08; fax: +1 508 457 23 10.
E-mail addresses: ilgar@virginia.edu (I. Safak), cisahin@ufl.edu (C. Sahin), jkaihatu@civil.tamu.edu (J.M. Kaihatu), alex@coastal.ufl.edu (A. Sheremet).

1463-5003/$ - see front matter © 2012 Elsevier Ltd. All rights reserved.
http://dx.doi.org/10.1016/j.ocemod.2012.11.006

boundary layer thickness of the mud layer, $\sqrt{\frac{2\nu_m}{\omega}}$ (ν_m is the kinematic viscosity of the fluid mud layer, and ω is the wave radian frequency), and much thinner than the overlaying water layer. This simplification results in explicit expressions of wave dissipation rate and, therefore, computational efficiency. In these three studies, peak mud-induced wave energy dissipation was noted to occur when h_o is the same order of magnitude as, but slightly larger than, $\sqrt{\frac{2\nu_m}{\omega}}$ (20% in Gade, 1958; 30% in Dalrymple and Liu, 1978; 50% in Ng, 2000).

Other mud rheologies have been used such as visco-elastic (Hsiao and Shemdin, 1980; Liu and Chan, 2007; Mei et al., 2010) and visco-plastic models (Mei and Liu, 1987; Chan and Liu, 2009). Recently, viscous mud formulations have been incorporated into wave models; the formulation of Gade (1958) was modified for directional wave fields in a phase-averaged model (Winterwerp et al., 2007), and the formulation of Ng (2000) was implemented in a phase-resolving nonlinear wave model (Kaihatu et al., 2007).

Although these studies have helped to quantify wave energy dissipation due to mud, they have generally assumed temporally-constant rheological properties for the mud layer. However, under wave forcing changing throughout a storm, rheology of a muddy seafloor is likely to vary. The complexity of observing the properties of muddy seafloors throughout wave-energetic periods precludes the direct evaluation of wave propagation in muddy environments and limits the applicability of wave-mud interaction formulations in operational wave models. Therefore, wave models have been recently used in an inverse manner in order to infer properties of mud layers that control frequency-dependent wave dissipation, such as thickness and viscosity. One initial inversion study was based on implementation of the model of Ng (2000) into SWAN (Rogers and Holland, 2009). The same mud dissipation formulation was implemented into nonlinear wave models (Sheremet et al., 2011a; Tahvildari and Kaihatu, 2011) with rigorous formulations of nonlinear triad interactions (Agnon and Sheremet, 1997; Kaihatu and Kirby, 1995) rather than the related parametrizations in SWAN. By comparing the results of linear and nonlinear models, Sheremet et al. (2011a) demonstrated the importance of accounting for nonlinear triad interactions in controlling the frequency distribution of wave energy dissipation. Their nonlinear model captured both the enhanced dissipation at the spectral peak due to energy transfers to higher and lower frequencies, and the resulting overall growth at these frequencies; neither effect is captured by linear wave transformation models (Agnon and Sheremet, 1997; Kaihatu et al., 2007; Elgar and Raubenheimer, 2008). This reveals that a nonlinear wave model is necessary in order to extract accurate properties of muddy seafloors in an inverse manner and, therefore, obtain a better representation of wave-mud interaction processes. Based on wave measurements collected nearby during a previous field effort (Section 3.1), Elgar and Raubenheimer (2008) developed a depth- and frequency-dependent formulation of mud-induced dissipation. The differences between the measured energy flux and estimates from a nondissipative nonlinear Boussinesq model were attributed to mud-induced dissipation only, with no allowances for other potential sources of dissipation (breaking, whitecapping, etc.). Despite the dependence on mud dissipation, no quantitative properties of the muddy seafloor were discussed or deduced from the data in their study.

In this study, we use wave, current, suspended sediment and seafloor observations to infer properties of the bottom mud layer. These measurements, taken along a cross-shelf transect on the muddy central chenier-plain coast, western Louisiana Shelf, United States during an energetic wave period (Section 3), are used herein to model wave propagation across the muddy seafloor and bottom boundary layer processes with two previously validated models. A nonlinear wave model (Agnon and Sheremet, 1997, Section 2.1) is used in an inverse manner to estimate evolution of viscosity of the muddy seafloor throughout the event of interest. The model used herein includes both mud induced (Ng, 2000) and breaking induced (Sheremet et al., 2011b) dissipation, therefore, distinguishes between these two mechanisms. Our approach follows Sheremet et al. (2011a) and is tested herein under different forcing conditions, as a step towards building a methodology to forecast bed reworking by waves. Compared to the study site used by Sheremet et al. (2011a), the study site herein is a plane shelf (Section 3.1) and better suited. In addition, near-bed conditions are investigated in more detail (sediment concentration, bottom shear stress) in this study. Measured profiles of acoustic backscatter are used to estimate vertical structure of suspended sediment concentration (Section 3.1, Appendix). These estimates are then used, together with the observed flow conditions, to run a bottom boundary layer model for muddy environments (Hsu et al., 2009, Section 2.2). Evaluation of the results of the wave model and the boundary layer model together allows to gain more insight into wave-mud interaction (Section 4).

2. Models

2.1. Nonlinear wave model

The spectral wave model is based on the nonlinear Mild Slope Equation and accounts for the interactions and spectral energy transfers among Fourier modes (Agnon et al., 1993; Agnon and Sheremet, 1997). The model is derived from the boundary value problem for water waves, with boundary conditions expanded to second order in ka, where k is the wavenumber and a a representative amplitude. The model thus describes both linear wave transformation effects and nonlinear wave–wave interactions; these interactions are expressed as coupled Fourier modes which govern the strength of the energy transfer. The phase-resolving evolution equations of this model are then averaged; the resulting equations represent the evolution of spectra in terms of bispectra. Bispectral evolution equations are then required, and the system truncated and closed. The 'sum' and 'difference' interactions represented in these coupled modes are associated respectively with the generation of both harmonics of the spectral peak and energy transfers toward lower frequencies, which impact processes in the nearshore environment (Sheremet et al., 2011a). The stochastic (phase-averaged) and unidirectional version of the model is modified to account for the dissipative processes. A mud-induced dissipation formulation that treats the fluid-mud layer as a viscous Newtonian fluid (Ng, 2000, Section 1) is used. The mud-induced dissipation rate is a function of wave frequency, mud thickness, density, and viscosity. Depth-induced breaking is represented with a lumped probability-based breaking mechanism (Thornton and Guza, 1983) with a ratio of breaking wave height to breaking depth, i.e., breaker index, of γ=0.7 and a breaking intensity parameter set to B = 1. The dissipation is assumed to be constant over the frequency range; this is expected to only affect predictions of third moment statistics (skewness and asymmetry) but not spectral levels (Chen et al., 1997). Energy input due to winds is not included given the relatively weak winds during the modeled period and small distance along the cross-shore transect considered. The dissipation effects are included in the spectral but not in the bispectral evolution. The resulting model is integrated to obtain the cross-shore evolution of the modal energy flux, accounting for nonlinear interactions, shoaling, and dissipation, represented by the net modal dissipation rate κ_j (see in Eq. (2) the net wave dissipation rate of flux integrated over the frequencies). See Appendix B

in Sheremet et al. (2011a) for the details of the use of the model, and Agnon and Sheremet (1997) for the derivation of the governing equations.

Given the observed spectral wave propagation and near-bed conditions, the wave model is used in an inverse manner to estimate the optimum mud properties from best fit between model and measurements. The optimization procedure involves a constrained nonlinear least squares minimization and allows to find the optimum viscosity of the mud layer that minimizes the following deviation:

$$\varepsilon = \sqrt{\frac{1}{SN}\sum_{i=1}^{S}\sum_{j=1}^{N}\frac{[F_m(f_j,x_i)-F(f_j,x_i)]^2}{F^2(f_j,x_i)}}, \quad (1)$$

where S is the number of sensors at which optimization is done by minimizing the errors in the spectral density estimates. Here, we use three sensors (S = 3, Section 3), an improvement over the single sensor used for inversion and optimization by Sheremet et al. (2011a). N is the number of Fourier modes, $F_m(f_j,x_i)$ is the energy flux predicted by the model at mode j with frequency f and at sensor i at cross-shore distance x, and F is the measured energy flux. Reference is made to Sheremet et al. (2011a) for the details of the optimization procedure.

2.2. Boundary layer model

A 1DV (one-dimensional vertical) boundary layer model that accounts for combined wave-current flow on muddy seafloors (Hsu et al., 2009) is used to deduce the near-bed conditions during the event of interest. The model integrates the two-phase (fluid and sediment) Reynolds-averaged Navier–Stokes equations; the turbulent flux terms in the equations are computed based on a turbulent kinetic energy-dissipation rate of turbulent kinetic energy closure. The momentum balance is between free-stream horizontal pressure gradient and momentum transport by viscous and turbulent shear stresses; the suspended sediment concentration balance is between turbulent mass flux and gravitational settling. The model accounts for the turbulence damping effect of sediment-induced stratification. In the model, the sediment phase is defined with a primary particle size (D_p), fractal dimension (n_f), critical shear stress to initiate sediment motion at the bed (τ_c), floc size (D_f), and a resuspension coefficient (γ_o), all of which are spatially and temporally constant within the model domain. In all the cases simulated, the first three parameters are set as $D_p = 5$ μm, n_f = 2.3, and τ_c = 0.4 Pa, based on the observations and results of the recent applications of this model on the Louisiana Shelf (Safak et al., 2010a; Sahin et al., 2012). Floc size and resuspension coefficient are varied as free calibration parameters to control sediment availability (Sahin et al., 2012). Resuspension coefficients of O (10^{-4}) and relatively small sensitivity of the model results to critical shear stress are found to be consistent with those used in the previous applications mentioned above (Safak et al., 2010a; Sahin et al., 2012). The application of the model to the data set, and how the flow conditions are prescribed are detailed in Section 4.2.

3. Field experiment

3.1. Site and instrumentation

The field experiment was conducted off the muddy central chenier-plain coast, western Louisiana Shelf at the northern Gulf of Mexico coast of the United States, about 100 km west of the Atchafalaya clinoform (Fig. 1). The eastern part of this mud rich coast was reported to prograde, despite relative sea level rise, due to net westward and onshore transport of Atchafalaya River sediment resuspended on the inner shelf (Draut et al., 2005a). The study site was at the western limit of the influence of the subaqueous delta formed by the Atchafalaya River sediment, and the proportion of the Atchafalaya River's sediment load that accumulates on the inner shelf seaward of the chenier-plain coast (Draut et al., 2005b). Early spring is the wave-energetic period of the Louisiana Shelf and the high-discharge period of the Atchafalaya River. In February-March 2008, four Acoustic Doppler Velocimeters (ADV, Sontek/YSI) were deployed along a cross-shelf transect. The mean depths at these sensor locations were 4.2, 3.75, 3.5, and 2.9 m; the sensor at the shallowest location was about 1.4 km off the coast (Fig. 2, Safak et al., 2010b). This cross-shore transect spanned about 1 km section, and the slope of the seafloor is about 0.1%. Net wave dissipation rate across the transect is calculated as:

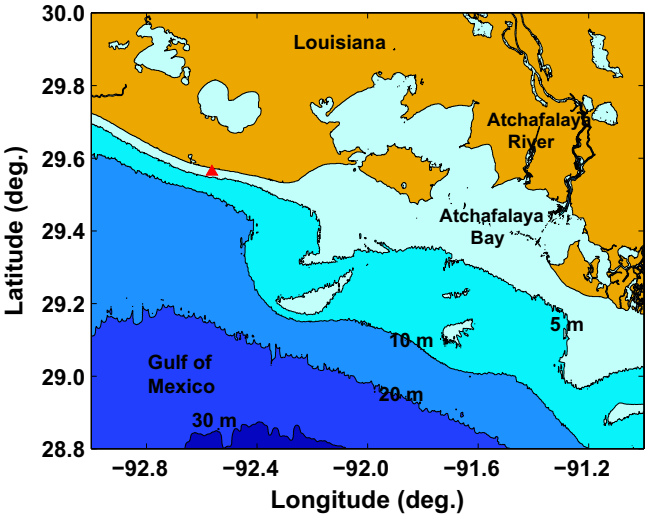

Fig. 1. Map of the Louisiana Shelf at the northern Gulf of Mexico. The red triangle marks the experiment location at the central chenier-plain coast. The sensor at the shallowest location was at 29.57 degrees North Latitude and 92.5617 degrees West Longitude. (For interpretation of the references to colour in this figure legend, the reader is referred to the web version of this article.)

$$\kappa = \frac{1}{\Delta x}\frac{F_i - F_{i+1}}{F_i}, \quad (2)$$

where Δx is the propagation distance between locations of interest, F is the measured energy flux integrated over $0.0039 \leqslant f \leqslant 0.3$ Hz (Fig. 3b), and subscript i denotes sensor number increasing onshore. To investigate wave direction, data from a Datawell directional buoy, 13 km offshore of the transect, were used. The buoy was deployed at 14 meter depth by Scripps Institution of Oceanography, Coastal Data Information Program (station 148; 29.4442 degrees North, 92.6324 degrees West).

ADVs sampled pressure and 3-D velocity at 2-Hz in 51 min intervals that were started every two hours at 92 cm above the seafloor at their locations. Within the transect, between ADVs 1 and 2 at about 4 m depth (Fig. 2), high-resolution observations of near-bed flows and sediment concentration were collected with a downward-pointing Pulse-Coherent-Acoustic Doppler Profiler (PC-ADP, Sontek/YSI). The PC-ADP was set to sample velocity and acoustic backscatter at 17 bins of 3.2 cm near the seafloor at 2-Hz in 10 min intervals every 20 min. The PC-ADP malfunctioned and did not return any velocity data. The acoustic backscatter signal of the PC-ADP is calibrated to estimate the vertical structure of suspended sediment concentration (Sahin et al., 2012); the calibration procedures are discussed in the Appendix. On the same platform, an OBS-3 and an OBS-5 (Optical Backscatterance Sensor, D&A Instruments), both of which were calibrated to give suspended

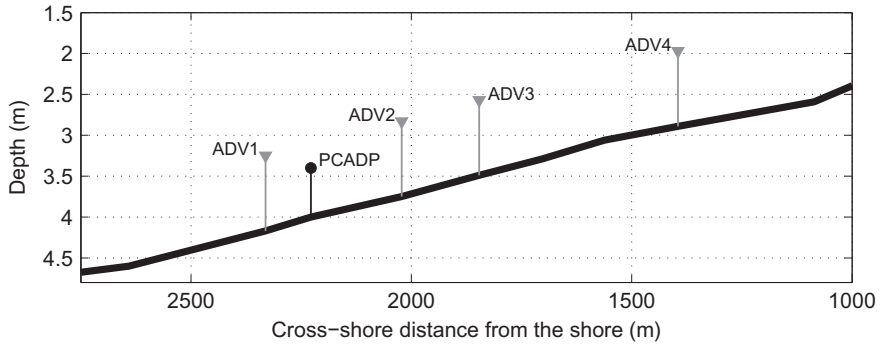

Fig. 2. Cross-shore transect of instruments, deployed during the experiment, that span about 1 km. Grey triangles indicate the approximate locations of the sensor volumes of the ADVs, black circle indicates the approximate location of the downward signal transmission of the PC-ADP.

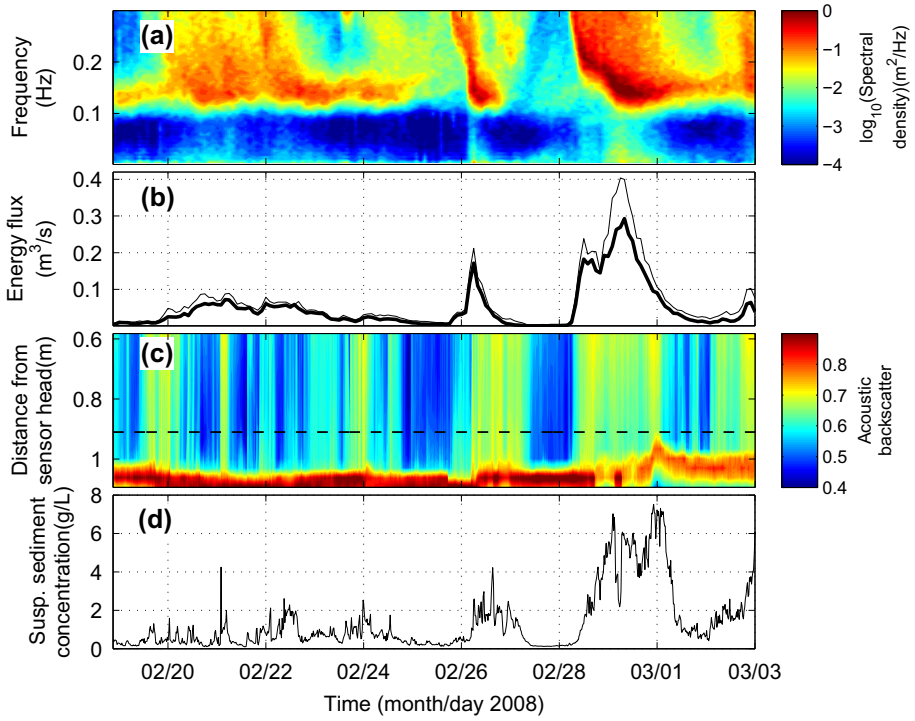

Fig. 3. Time evolution of: (a) power spectral density of sea surface elevation, (b) frequency-integrated ($0.0039 \leqslant f \leqslant 0.3$ Hz) wave energy flux at sensors ADV-1 (thin line, 4.2 m depth) and ADV-4 (thick line, 2.9 m depth); (c) vertical structure of the PC-ADP acoustic backscatter, normalized by the maximum of the measured backscatter; and (d) suspended sediment concentration measured at the level indicated by the dashed line in panel (c). (For interpretation to colours in this figure, the reader is referred to the web version of this paper.)

sediment concentration, were also deployed to measure turbidity. The OBS-3 sampled at 18 cm above bed in synchronization with the PC-ADP; the OBS-5, which returned one averaged sample every 10 min at 12 cm above bed, ran out of power on February 28th and provided data only for the first 10 days of the experiment.

3.2. Observations

The event studied here was selected because a combination of factors (forcing strength, bed behavior) led to the demonstration of a clear connection between surface wave dissipation and mud characteristics. Observations of the wave and near-bed conditions (comprising a two-week period) are summarized in Fig. 3. Wave energy is decomposed into sea (short-wave, $0.2 < f \leqslant 0.3$ Hz), swell ($0.05 < f \leqslant 0.2$ Hz), and infragravity waves ($f \leqslant 0.05$ Hz) bands. In the first half of the experiment, wave energy and near-bed activity were relatively small (see the relatively steady maximum backscatter location in Fig. 3c). Following a relatively short duration wave event on February 26th (Fig. 3a and b), wave energies at all three bands reached their maxima during the experiment on February 29th (Fig. 3a) within a two-day long event. The spectral peak period remained near 7 s for one day (Fig. 3a). This increase in wave energy triggered seafloor response and near-bed activity; this is most apparent on March 1st from the significant variation of the maximum backscatter location (Fig. 3c) and near-bed sediment concentrations exceeding 7 g/L (Fig. 3d).

Fig. 4 presents a closer look at the observations during the time of the more energetic events, the last three-day period of which is the focus of wave and boundary layer modeling (29 February–2 March 2008). Wind data from a weather station located on the Atchafalaya inner shelf indicate that winds during this event of modeling interest were relatively weak (average speed of 4 m/s); they were directed northward for the first 18-h period and then mostly westward during the next two days. Currents were O (10 cm/s), and consistently westward (Fig. 4a). The westward currents, which coincide with the high sediment concentrations

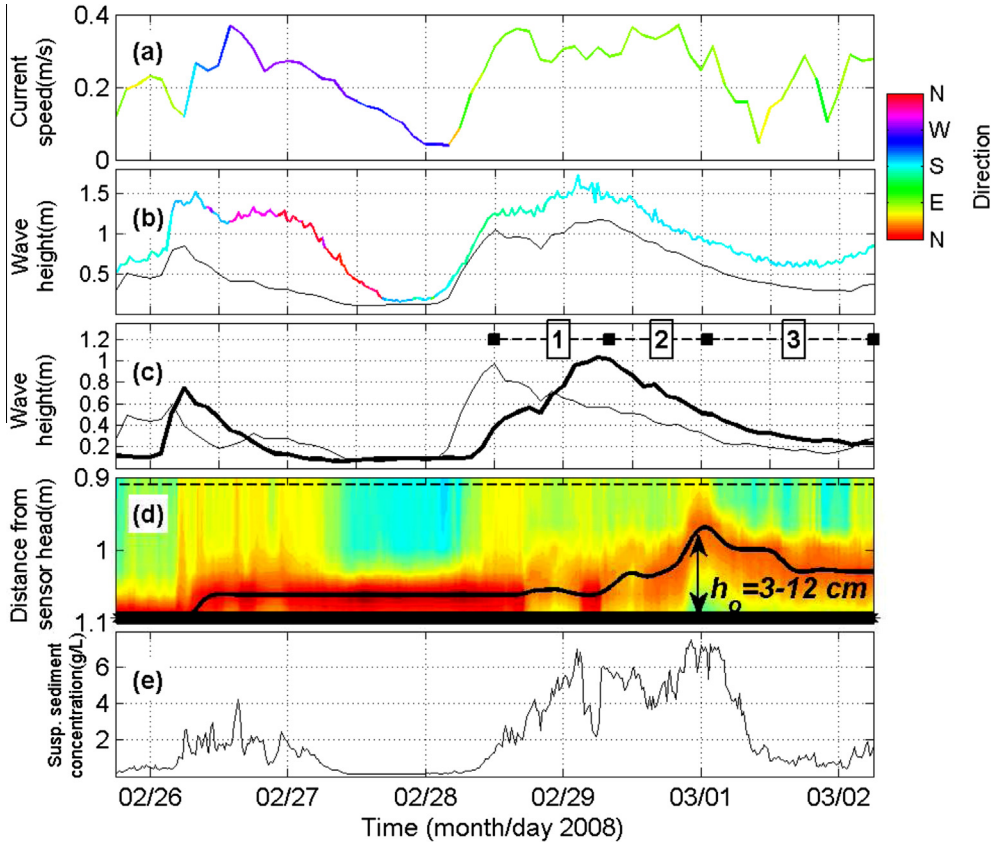

Fig. 4. Time evolution of: (a) mean current speed measured by ADV-1 at 4.2 m depth (color code indicates where the currents are coming from); (b) total significant wave height measured at the SIO-CDIP buoy at about 13 km offshore of the cross-shore transect (color code indicates where the waves are coming from) and at ADV-1 (black curve); (c) significant wave height at the sea (thin line, $0.2 < f \leqslant 0.3$ Hz) and swell (thick line, $0.05 < f \leqslant 0.2$ Hz) bands measured by ADV-1; (d) vertical structure of the PC-ADP acoustic backscatter at the lowest 20 cm near the seafloor, normalized by the maximum of the measured backscatter (red and blue correspond to high and low backscatter, respectively); and (e) suspended sediment concentration measured at the level indicated by the dashed line in panel (d). In panel (d), the curve shows the moving average of the location of the maximum backscatter which is assumed to be the lutocline and the upper limit of the fluid mud layer; thick line denotes the level of the platform foot. '1', '2', and '3' in panel (c) correspond to the intervals during which wave energy is increasing on the initially consolidated seafloor, fluid mud thickness is increasing due to decrease in wave energy, and settling of the initially resuspended material and consolidation of the fluid mud layer, respectively. (For interpretation of the references to colour in this figure legend, the reader is referred to the web version of this article.)

recorded (Fig. 4e), are believed to be responsible for advection of Atchafalaya River sediment to the chenier-plain coast (Wells and Kemp, 1981; Allison et al., 2000; Kineke et al., 2006). Fig. 4b shows mean wave direction measured at the offshore buoy and significant wave heights measured at the offshore buoy and the sensor at the deepest location at the transect. The directions measured at 13 km offshore of the transect indicate that waves were mostly from the south (almost perpendicular to the shore) for the vast majority of the interval shown, except during a one-day period around February 27th, when waves were from the north. As it might be expected, the trends of wave heights measured at the buoy and at the transect (Fig. 4b) agree well. The level of maximum acoustic backscatter is assumed to be the lutocline, the location of a sharp gradient in concentration and density (black curve in Fig. 4d). The distance between the lutocline elevation (Fig. 4d) and the level of the platform foot is assumed to be the fluid mud thickness. The correlation between the lutocline elevation (Fig. 4d), sediment concentrations (Fig. 4e), swell energy (thick curve in Fig. 4c), and westward currents (Fig. 4a) is evident. The shorter and weaker event on February 26th, with swells exceeding 0.7 m height, caused a relatively small seafloor response. During the period indicated with '1' in Fig. 4c, swells increasing up to 1 meter significant height (with peak period of 7 s) and westward currents exceeding 35 cm/s (Fig. 4a) caused sediment resuspension (Fig. 4e). After swells started to lose energy ('2' in Fig. 4c), measured suspended sediment concentration stayed relatively steady, however, the increasing fluid mud thickness (as high as 12 cm, Fig. 4d) suggests an expected downward sediment flux within the water column. Once the swell energy dropped below a threshold value (corresponding to about 0.5 m height), observations suggest a rapid settling throughout the water column and also start of the consolidation of the mud layer ('3' in Fig. 4d). Overall, the estimated thickness of the mud layer varied between 3–12 cm throughout this event; these estimates are used as the inputs of the mud-induced dissipation formulation in the wave model (Section 4.1).

4. Results

4.1. Nonlinear wave model

The wave model is initialized at ADV-1 (sensor at the deepest location), with the wave spectrum discretized into 77 Fourier modes, the maximum frequency of which is 0.3 Hz. The thickness of the fluid mud layer is estimated from the near-bed vertical structure of acoustic backscatter (3–12 cm, Fig. 4d, Section 3.2); this is used in the mud-induced dissipation mechanism implemented in the wave model (Ng, 2000). Based on the results of the laboratory experiments of wave forcing on mud samples

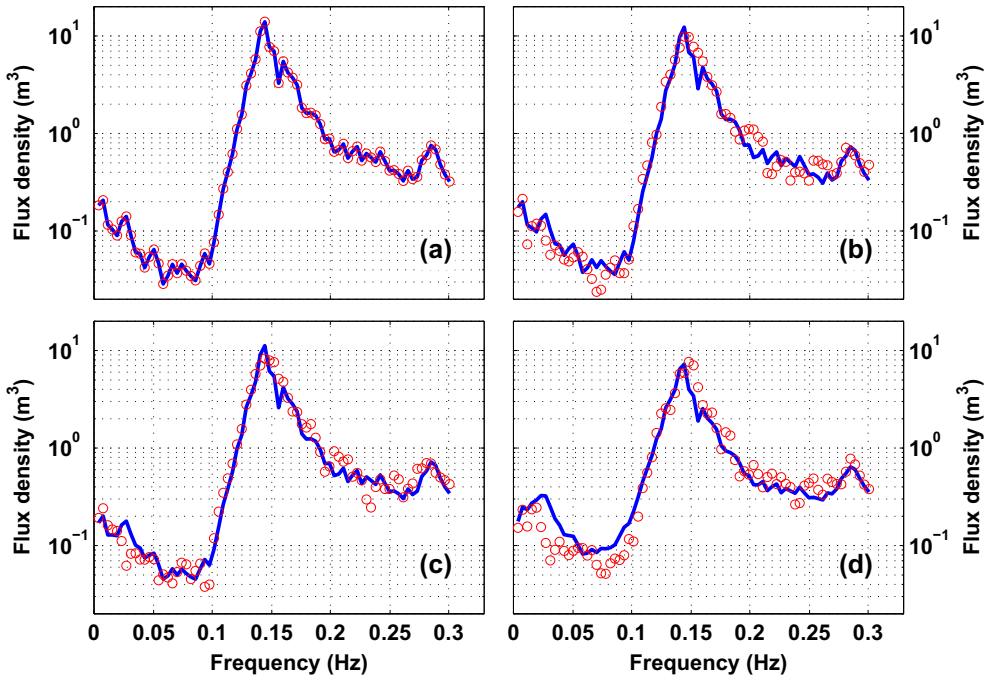

Fig. 5. Comparison of model calculations of flux density with the one obtained from the data, for the burst starting at February 29th, 08:00 (with swell height of about 1 m, which was the highest during the modeled interval) at sensors (a) ADV-1, (b) ADV-2, (c) ADV-3, and (d) ADV-4. Blue lines denote model calculations and red circles denote estimates based on the measurements. Optimized kinematic viscosity of the fluid mud layer for this case is $\nu_m = 1.48 \times 10^{-4}$ m^2/s. (For interpretation of the references to colour in this figure legend, the reader is referred to the web version of this article.)

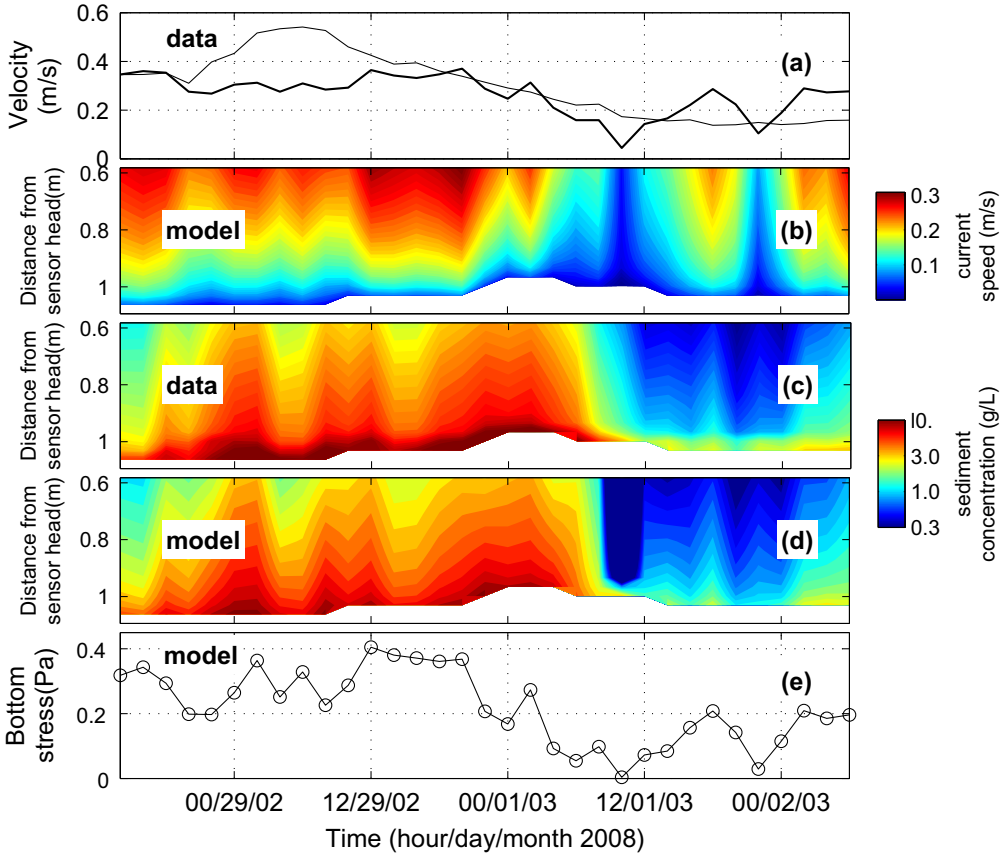

Fig. 6. Results of the boundary layer model. Time evolution of (a) mean current speed (thick line) and wave-induced velocity corresponding to the measured variance of the velocities (thin line) measured at ADV-1; (b) model calculations of current speed; (c) estimates of suspended sediment concentration, based on calibration of the PC-ADP acoustic backscatter; (d) model calculations of suspended sediment concentration; and (e) bottom shear stress calculations of the model. (For interpretation to colours in this figure, the reader is referred to the web version of this paper.)

collected on the Atchafalaya Shelf (Robillard, 2009), a direct proportion between the fluid mud density (ρ_m, varying between 1025–1350 kg/m^3) and the fluid mud kinematic viscosity (ν_m, varying between 10^{-6}–10^{-1} m^2/s) is used to relate these two quantities (Sheremet et al., 2011a). The only mud-related parameter left to calibrate is the fluid mud viscosity. This parameter is varied between 10^{-6}–10^{-1} m^2/s in order to find its optimum value that yields the best fit between observed and modeled spectra at frequencies $f > 0.1$ Hz. The accuracy of the algorithm can be seen in the comparison of the data and the model results (Fig. 5). Using this methodology, estimates of the optimum fluid mud viscosity are found to vary more than one order of magnitude throughout the event of interest (Section 4.3). The optimum model estimates of mud viscosity were then included in the analysis of the observations and the results of bottom boundary layer modeling.

4.2. Boundary layer model

Due to absence of velocity data from the PC-ADP, the bottom boundary layer model is forced with the velocities measured at ADV-1, the closest to the PC-ADP (Fig. 2). No significant difference is observed between the statistics of the velocity measured at ADVs 1 and 2. The top and bottom boundaries of the model are set at 92 cm above bed, and the location of the maximum acoustic backscatter, respectively; the former corresponds to the location of the ADV measurements. Input for mean current flow in the boundary layer is specified in the model by assuming a logarithmic velocity profile (modified in the model due to presence of waves and suspended-sediment-induced stratification) with an average bottom roughness of $z_o = 3$ cm (Sahin et al., 2012), and fitting the observed mean current at the top model boundary. The oscillatory part of the flow is prescribed with a sinusoidal wave with the spectral peak frequency and an amplitude corresponding to the variance obtained from the velocity measurements. The 'relaxation time' method (Hsu et al., 2009) adjusts the pressure gradient term in the horizontal momentum equation for a given depth-averaged velocity (Winterwerp and van Kesteren, 2004), is used due to the large number of cases modeled and the corresponding need for expedient computation. Fig. 6a shows the model forcing of mean current (thick line) and amplitude of sinusoidal wave velocity (thin line), the latter of which largely follows the swell wave height (Fig. 4c); Fig. 6b shows the mean current profiles the model generates. The agreement of the model with the estimates of vertical structure of suspended sediment concentration is favorable (Fig. 6c and d); the normalized root-mean-square error of the model calculations of sediment concentration is between 5–18%, with an average of 9%. Results suggest that near-bed sediment concentrations exceeded 10 g/L (Fig. 6c and d). The similarity in trends of sediment concentration and bottom stress is evident (Fig. 6e). With the sudden drop in bottom stress at the end of February 29th, sediment concentration throughout the water column started to decrease. On March 1st, 08:00, when the bottom stress was about 0.1 Pa, the concentrations in the water column were decreasing to values less than O (1 g/L). Overall, the computed bottom shear stress varies between 0.03–0.4 Pa (Fig. 6e). Model-data agreement is poor during the two hour interval at 10:00 on March 1st (Fig. 6c and d). This corresponds to a settling event due to relatively weak flow (both currents and waves, Fig. 6a), therefore, the turbulence generated in the model is not able to maintain the estimated sediment concentrations.

4.3. Summary of the event

Fig. 7 summarizes the observed conditions and the model results of fluid mud viscosity during the event of interest. Initially, the swell wave energy was relatively small (Fig. 7a), the seafloor was likely to be consolidated (Fig. 7b), and the viscosity of the fluid mud layer (estimated from inverse wave modeling) was the maximum for

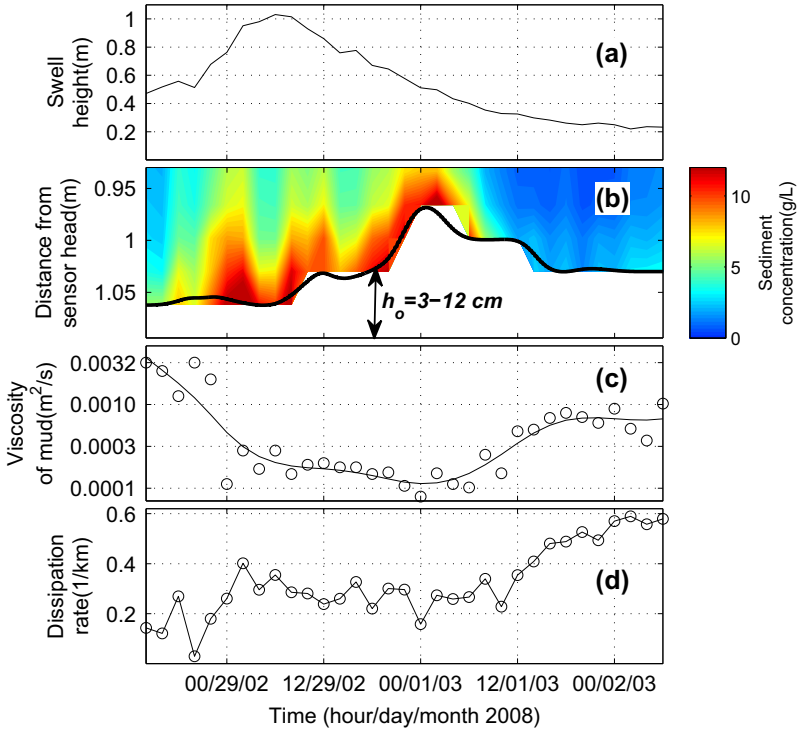

Fig. 7. Time evolution of: (a) significant wave height at the swell band ($0.05 < f \leqslant 0.2$ Hz) measured by ADV-1 at 4.2 m depth; (b) estimates of near-bed suspended sediment concentration (black curve indicates the moving average of the location of maximum backscatter, i.e., lutocline); (c) estimates of fluid mud layer viscosity, obtained from inverse wave modeling (shown in a logarithmic scale; the curve indicates the moving average); and (d) net wave energy dissipation rate, based on energy flux integrated over frequency, between ADV-1 (4.2 m depth) and ADV-4 (2.9 m depth) that were separated by 940 m. (For interpretation to colours in this figure, the reader is referred to the web version of this paper.)

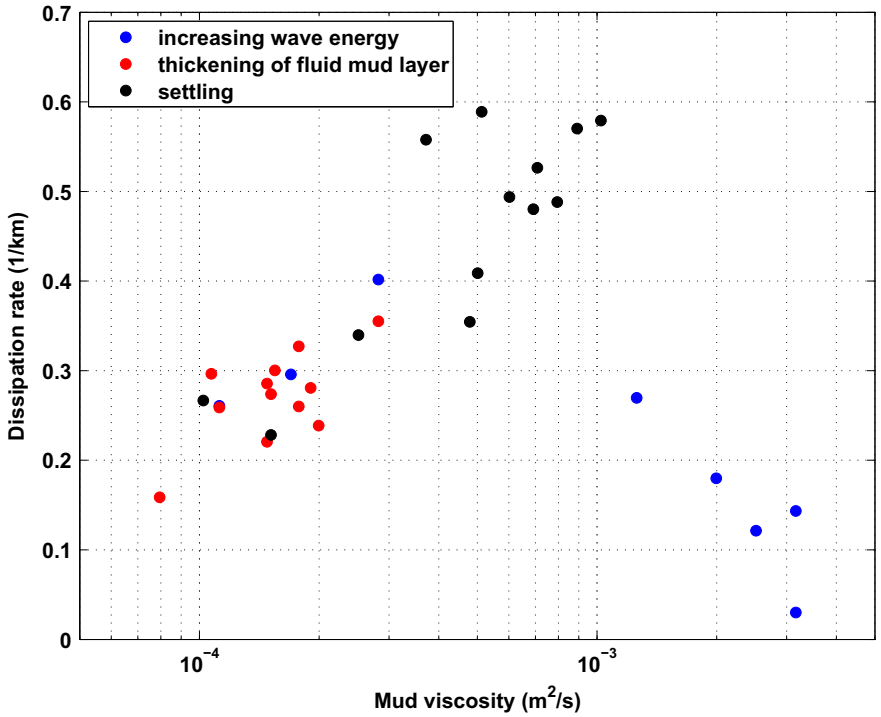

Fig. 8. Variation of the model estimates of the kinematic viscosity of the fluid mud layer with the observed rate of wave energy dissipation. Blue, red and black circles correspond to the intervals during which wave energy is increasing on the initially consolidated seafloor, fluid mud thickness is increasing due to decrease in wave energy, and settling of the initially resuspended material and consolidation of the fluid mud layer, respectively, i.e., '1', '2', and '3' in Fig. 4c. (For interpretation to colours in this figure, the reader is referred to the web version of this paper.)

the modeled interval ($10^{-2.5}$ m^2/s, Fig. 7c). An increase in swell energy between the beginning of the modeled interval and February 29th, 08:00 (Fig. 7a) augmented the near-bed sediment concentrations (Fig. 7b). This increase in swell energy also softened the seafloor, indicated by a decrease in viscosity of more than one order of magnitude (Fig. 7c). As swells were losing energy after February 29th, 08:00 (Fig. 7a), and bottom stresses were decreasing after 12:00 (Fig. 6e), thickness of the fluid mud layer increased until March 1st, 00:00 (Fig. 7b). Fluid mud viscosity was still decreasing during this interval, but at a smaller rate, and the values were O (10^{-4} m^2/s) (Fig. 7c). After March 1st, 00:00, as swell energy decreased even further (Fig. 7a, see also the decreasing current speed and bottom stress in Figs. 6a and e), settling occurred in the water column and fluid mud layer started to consolidate (Fig. 7b). The fluid mud viscosity reached O (10^{-3} m^2/s), a value smaller than the estimates at the beginning of the modeled interval (Fig. 7c). This increase in viscosity during the settling period is in agreement with the trend of the viscosity estimates for the settling period modeled by Sheremet et al. (2011a). The range of fluid mud viscosity estimated from the model is $10^{-4.1}$–$10^{-2.5}$ m^2/s; corresponding fluid mud density range is 1080–1210 kg/m^3 which is within the range of density of occurrence of fluid mud (Jain and Mehta, 2009; Sahin et al., 2012). Viscosity estimates higher than those obtained on the Atchafalaya Shelf (Sheremet et al., 2011a) suggest a different response of mud to waves. This could be attributed to different forcing conditions and local geology. The event studied herein is less energetic with smaller wave heights and periods, and relatively short. Although the major sediment source of the study site is the Atchafalaya Shelf, the cycles of resuspension/deposition of sediment during westward advection from the shelf, resulting lower long term accumulation rates at the study site, and the effect of local relict material may cause the differences in the response of fluid mud to waves, i.e., viscosity of the fluid mud layer. The net wave dissipation rate across the transect (Eq. (2), Δx = 940 m between ADV-1 and ADV-4) shows an overall increasing trend throughout the modeled interval (Sheremet et al., 2011a), especially after the start of settling throughout the water column and consolidation of the fluid mud layer (March 1st, 00:00, Fig. 7b), and reaches its maximum in the end (Fig. 7d). Therefore, the most efficient mud-induced dissipation was observed when the resuspended sediment settled into a fluid mud layer that has a thickness and a viscosity (black circles in Fig. 8) between those that are associated with an initially consolidated seafloor (small thickness and large viscosity, blue circles in Fig. 8) and a high concentration layer formed due to strong wave action (large thickness and small viscosity, red circles in Fig. 8). The net dissipation rates observed (mostly 0.2–0.6 km^{-1}) are of the same order of magnitude as those observed by Elgar and Raubenheimer (2008) close to the present study site (see the dissipation rates within 3–4 m depth range in Fig. 2 in their study) and Sheremet et al. (2011a) on the Atchafalaya inner shelf.

5. Conclusions

Interaction of surface waves with a muddy seafloor on a shallow, mild-slope (0.1%) shelf was studied with field measurements of flow and near-bed conditions along a 1 km transect (average water depth of 3.5 m), and modeled with a spectral wave model and a bottom boundary layer model for muddy seafloors. The wave model accounts for nonlinear energy transfers across spectrum, which were shown to be essential in investigation of frequency-dependent mud-induced dissipation of waves (Sheremet et al., 2011a). The model was used in an inverse manner (Rogers and Holland, 2009; Sheremet et al., 2011a; Tahvildari and Kaihatu, 2011) in order to estimate the viscosity of the fluid mud layer which is a key parameter that controls mud-induced wave dissipation.

Observations suggested a strong coupling between flow (waves and currents) and near-bed fluid mud layers. Estimates of vertical

structure of sediment concentration and boundary layer model computations of near-bed flow parameters that are not directly available (e.g., bottom shear stress) have been included first time in a wave-mud interaction study to infer about bed properties during a wave event. By using these observations, estimates and the model results, the event of interest could be divided into three stages that support the previous findings: (i) resuspension due to high bottom shear stresses and increasing swell energy, (ii) thickening of the fluid mud layer due to decline in wave energy, and (iii) settling of resuspended sediment, and start of consolidation of the fluid mud layer as swell energy and bottom shear stress decrease further. The near-bed concentrations observed were as high as 12 g/L, which is of the same order of magnitude as the conventionally accepted limit of fluid mud (Mehta, 1989; Winterwerp and van Kesteren, 2004). The most substantial dissipation effect of the fluid mud layer (with dissipation rates of the same order of magnitude as those reported in nearby locations, Elgar and Raubenheimer (2008); Sheremet et al. (2011a)) was observed when the resuspended sediment settled to form a fluid mud layer. This is in agreement with the observations and model results of Sheremet et al. (2011a). The mud viscosities estimated during this peak-dissipation interval are smaller than those estimated for the initially consolidated bed, and higher than those estimated for the mud layer that is likely to be soft during the strong wave action. The fluid mud layer properties, even by assuming a simple viscous rheology, were shown to vary an order of magnitude throughout a wave event. As it might be expected, estimates of viscosity of the fluid mud layer in the central chenier-plain coast were higher than those obtained under more energetic conditions on the Atchafalaya Shelf (Sheremet et al., 2011a) which experiences higher long term accumulation rates. Therefore, assuming a constant representation for fluid mud layers under different forcing conditions and coastal settings may be misleading. The effect of wave direction was not included in this study, to which model overestimation of wave energy at infragravity band is attributed (Fig. 5d); further work will concentrate on this topic.

Acknowledgments

This study was supported by the Office of Naval Research funding of contracts N00014-10-1-0363, N00014-10-1-0389, N00014-10-1-0805 and N00014-11-1-0269. We would like to thank Drs. Steve Elgar and Britt Raubenheimer from Woods Hole Oceanographic Institution for generously providing the access to the wave data set. Dr. Tian-Jian Hsu from the University of Delaware kindly provided the boundary layer model. The authors are grateful to Dr. Mead A. Allison from the University of Texas, the three anonymous reviewers and the guest editor Dr. Hendrik L. Tolman for their insightful and constructive comments.

Appendix A. Calibration of PC-ADP backscatter

The calibration involves estimation of a PC-ADP 'system constant', and search for an optimized, depth-independent, 'effective' floc size that yields the best agreement between concentrations measured by an independent instrument (OBS, herein) and PC-ADP estimates. The acoustic backscatter is corrected for spherical spreading, and attenuation due to water and sediment (Thorne and Hanes, 2002). The system constant was shown to be insensitive to floc size (Sahin et al., accepted for publication); therefore, a constant floc size of 200 μm, the common peak of size distribution data collected on the Louisiana Shelf under varying conditions (Safak, 2010; Safak et al., 2012), is used for estimation of the system constant. Once the system constant is determined, floc size that gives the best agreement between the estimated and measured concentrations is searched in the range of 50–350 μm, based on the previous floc size measurements (Safak, 2010; Safak et al., 2012). The reader is referred to Sahin et al. (accepted for publication) and Sahin et al. (2012) for further details of the calibration procedure. The calibration is done by using the data collected between 19–28 February, during which the two OBSs provided sediment concentration at two vertical levels within the profiling range of the PC-ADP. The vertical structure of suspended sediment concentration is estimated for the event of interest. The estimates from three PC-ADP measurement intervals of 10 min starting every 20 min, coinciding with each ADV measurement interval of 51 min starting every two hours, are averaged to obtain one vertical profile of sediment concentration for each ADV measurement interval. The average normalized root-mean square error between estimates and measurements is 13%, with a correlation coefficient of $r^2 = 0.97$.

References

Agnon, Y., Sheremet, A., 1997. Stochastic nonlinear shoaling of directional spectra. J. Fluid Mech. 345, 79–99.
Agnon, Y., Sheremet, A., Gonsalves, J., Stiassnie, M., 1993. Nonlinear evolution of a unidirectional shoaling wave field. Coast. Eng. 20, 29–58.
Allison, M.A., Kineke, G.C., Gordon, E.S., Goni, M.A., 2000. Development and reworking of a seasonal flood deposit on the inner continental shelf off the Atchafalaya River. Cont. Shelf Res. 20, 2267–2294.
Ardhuin, F., O'Reilly, W.C., Herbers, T.H.C., Jessen, P.F., 2003. Swell transformation across the continental shelf. Part 1: Attenuation and directional broadening. J. Phys. Oceanogr. 33 (9), 1921–1939.
Chan, I.-C., Liu, P.L.-F., 2009. Responses of Bingham-plastic muddy seabed to a surface solitary wave. J. Fluid Mech. 618, 155–180.
Chen, Y., Guza, R.T., Elgar, S., 1997. Modeling spectra of breaking surface waves in shallow water. J. Geophys. Res. 102 (C11), 25035–25046.
Dalrymple, R.A., Liu, P.L.-F., 1978. Waves over soft mud: a two-layer fluid model. J. Phys. Oceanogr. 8, 1121–1131.
Draut, A.E., Kineke, G.C., Kuh, O.K., Grymes III, J.M., Westphal, K.A., Moeller, C.C., 2005a. Coastal mudflat accretion under energetic conditions, Louisiana chenier-plain coast, USA. Mar. Geo. 214, 27–47.
Draut, A.E., Kineke, G.C., Velasco, D.W., Allison, M.A., Prime, R.J., 2005b. Influence of the Atchafalaya River on recent evolution of the chenier-plain inner continental shelf, northern Gulf of Mexico. Cont. Shelf Res. 25, 91–112.
Elgar, S., Raubenheimer, B., 2008. Wave dissipation by muddy seafloors. Geophys. Res. Lett. 35, L07611. http://dx.doi.org/10.1029/2008GL033245.
Gade, H.G., 1958. Effects of a nonrigid, impermeable bottom on plane surface waves in shallow water. J. Mar. Res. 16, 61–82.
Hsiao, S.V., Shemdin, O.H., 1980. Interaction of ocean wave with a soft bottom. J. Phys. Oceanogr. 10, 605–610.
Hsu, T.-J., Ozdemir, C.E., Traykovski, P.A., 2009. High-resolution numerical modeling of wave-supported gravity driven mudflows. J. Geophys. Res. 114 (C5). http://dx.doi.org/10.1029/2008JC005006.
Jain, M., Mehta, A.J., 2009. Role of basic rheological models in determination of wave attenuation over muddy seabeds. Cont. Shelf Res. 29, 642–651.
Jaramillo, S., Sheremet, A., Allison, M.A., Reed, A.H., Holland, K.T., 2009. Wave-mud interactions over the muddy Atchafalaya subaqueous clinoform, Louisiana, United States: wave-supported sediment transport. J. Geophys. Res. 114 (C04002). http://dx.doi.org/10.1029/2008JC004821.
Kaihatu, J.M., Kirby, J.T., 1995. Nonlinear transformation of waves in finite water depth. Phys. Fluids 7, 1903–1914.
Kaihatu, J.M., Sheremet, A., Holland, K.T., 2007. A model for the propagation of nonlinear surface waves over viscous muds. Coast. Eng. 54, 752–764.
Kineke, G.C., Higgins, E.E., Hart, K., Velasco, D., 2006. Fine sediment transport associated with cold-front passages on the shallow shelf, Gulf of Mexico. Cont. Shelf Res. 26, 2073–2091.
Liu, P.L.-F., Chan, I.-C., 2007. A note on the effects of a thin visco-elastic mud layer on small amplitude water-wave propagation. Coast. Eng. 54, 233–247.
Mehta, A.J., 1989. On estuarine cohesive sediment suspension behaviour. J. Geophys. Res. 94, 14303–14314.
Mei, C.-C., Liu, K.-F., 1987. A Bingham-plastic model for a muddy seabed under long waves. J. Geophys. Res. 92, 14581–14594.
Mei, C.-C., Krotov, M., Huang, Z., Huhe, A., 2010. Short and long waves over a muddy seabed. J. Fluid Mech. 643, 33–58.
Ng, C.-N., 2000. Water waves over a muddy bed: a two-layer Stokes' boundary layer model. Coast. Eng. 40, 221–242.
Robillard, D.J., 2009. A laboratory investigation of mud seabed thickness contributing to wave attenuation. Ph.D. Dissertation, University of Florida, Gainesville, FL. <http://purl.fcla.edu/fcla/etd/UFE0024823>.
Rogers, W.E., Holland, K.T., 2009. A study of dissipation of wind-waves by mud at Cassino Beach, Brazil: prediction and inversion. Cont. Shelf Res. 29, 676–690.
Safak, I., 2010. Interaction of bottom turbulence and cohesive sediment on the muddy Atchafalaya Shelf, Louisiana, USA. Ph.D. Dissertation, University of Florida, Gainesville, FL. <http://purl.fcla.edu/fcla/etd/UFE0042017>.

Safak, I., Sheremet, A., Allison, M.A., Hsu, T.-J., 2010a. Bottom turbulence on the muddy Atchafalaya Shelf, Louisiana, USA. J. Geophys. Res. 115. http://dx.doi.org/10.1029/2010JC006157.

Safak, I., Sheremet, A., Elgar, S., Raubenheimer, B., 2010b. Nonlinear wave propagation across a muddy seafloor. Abstract P014B-03, EOS, Trans. AGU 91, presented at 2010 Ocean Sciences Meeting, Portland, Oregon, 22–26 February.

Safak, I., Allison, M.A., Sheremet, A. Floc variability under changing turbulent stresses and sediment availability on a wave energetic muddy shelf, Cont. Shelf Res. http://dx.doi.org/10.1016/j.csr.2012.11.015.

Sahin, C., Safak, I., Sheremet, A., Mehta, A.J., 2012. Observations on cohesive bed reworking by waves: Atchafalaya Shelf, Louisiana, USA. J. Geophys. Res. http://dx.doi.org/10.1029/2011JC007821.

Sahin, C., Safak, I., Hsu, T.-J., Sheremet, A., Observations of suspended sediment stratification from acoustic backscatter in muddy environments, Mar. Geol. accepted for publication.

Sheremet, A., Stone, G.W., 2003. Observations of nearshore wave dissipation over muddy sea beds. J. Geophys. Res. 108 (C11). http://dx.doi.org/10.1029/2003JC001885.

Sheremet, A., Mehta, A.J., Liu, B., Stone, G.W., 2005. Wave-sediment interaction on a muddy inner shelf during Hurricane Claudette. Estuar. Coast. Shelf Sci. 63, 225–233.

Sheremet, A., Jaramillo, S., Su, S.-F., Allison, M.A., Holland, K.T., 2011a. Wave-mud interactions over the muddy Atchafalaya subaqueous clinoform, Louisiana, USA: wave processes. J. Geophys. Res. 116 (C06005). http://dx.doi.org/10.1029/2010JC006644.

Sheremet, A., Kaihatu, J.M., Su, S.-F., Smith, E.R., Smith, J.M., 2011b. Modeling of nonlinear wave propagation over fringing reefs. Coast. Eng. 58, 1125–1137.

Tahvildari, N., Kaihatu, J.M., 2011. Optimized determination of viscous mud properties using a nonlinear wave-mud interaction model. J. Atmos. Ocean. Tech. 28, 1486–1503.

Thorne, P.D., Hanes, D.M., 2002. A review of acoustic measurement of small-scale sediment processes. Cont. Shelf Res. 22, 603–632.

Thornton, E.B., Guza, R.T., 1983. Transformation of wave height distribution. J. Geophys. Res. 88 (10), 5925–5938.

Wells, J.T., Kemp, G.P., 1981. Atchafalaya mud stream and recent mudflat progradation: Louisiana chenier plain. Gulf Coast Assoc. Geol. Soc. Trans. 31, 409–416.

Winterwerp, J.C., van Kesteren, W.G.M., 2004. Introduction to the physics of cohesive sediment in the marine environment. In: van Loon, T. (Ed.), Developments in sedimentology, vol. 56. Elsevier, Amsterdam, p. 66 pp.

Winterwerp, J.C., de Graaff, R.F., Groeneweg, J., Luijendijk, A.P., 2007. Modelling of wave damping at Guyana mud coast. Coast. Eng. 54, 249–261.